The Canadian Mineralogist
Vol. 37, pp. 559-573 (1999)

TELLURIDES FROM THE PALEOPROTEROZOIC OMAI GOLD DEPOSIT, GUIANA SHIELD

GABRIEL VOICU§

Département des Sciences de la Terre, Université du Québec à Montréal, C.P. 8888, Succ. Centre-Ville, Montréal, Québec H3C 3P8, Canada and Omai Gold Mines Limited, P.O. Box 12249, Georgetown, Guyana

MARC BARDOUX AND MICHEL JÉBRAK

Département des Sciences de la Terre, Université du Québec à Montréal, C.P. 8888, Succ. Centre-Ville, Montréal, Québec H3C 3P8, Canada

ABSTRACT

The Omai deposit, a Paleoproterozoic gold-bearing vein system, is located in the Barama–Mazaruni Supergroup, a typical greenstone belt in north-central Guyana. The deposit is hosted mainly by a shallow-level quartz-monzodioritic stock (Omai stock), quartz–feldspar porphyry and rhyolite dykes, and, to a lesser extent, by adjacent mafic volcanic and sedimentary rocks. In the Omai stock, the gold-bearing quartz veins show an uniform pattern, generally striking 030° and dipping at 20–30°. The veins hosted by the quartz–feldspar porphyries and rhyolites are stockworks. The metallic minerals (<2% of the vein volume) have a complex mineralogy consisting of various sulfides, associated with native elements, tungstates, tellurides, and sulfosalts. Telluride minerals are petzite, calaverite, hessite, tellurobismuthite, altaite, melonite, coloradoite, and volynskite. The metal inventory is defined by the Au–Ag–Te–W–Bi–Pb–Zn–Cu–Hg–Mo assemblage, characteristic of both epi- and mesothermal deposits. The gangue includes mainly quartz, with minor amounts of ankerite, calcite, albite, white mica, chlorite, and epidote. The conditions of ore formation at Omai are estimated from the stability of telluride – sulfide – oxide – silicate assemblages. The bulk of ore minerals and gangue precipitated at low temperatures (220° to 170°C), whereas solutions are characterized by relatively narrow ranges in S_2 (10^{-17} to 10^{-11}), Te_2 (10^{-14} to $10^{-10.5}$) and O_2 (10^{-43} to 10^{-36}) fugacities and a weakly acidic pH (between 4 and 5.4). Gold was probably transported as sulfide [$Au(HS)_2^-$ and $Au(HS)^0$ or $HAu(HS)_2^0$] or thiosulfate complexes, whereas Te was transported as aqueous H_2TeO_3, Te_2^{2-}, and HTe^- complexes.

Keywords: Omai gold deposit, Guiana Shield, tellurides, Te_2, S_2 and O_2 fugacities, pH, electron- microprobe analyses.

SOMMAIRE

Le gîte aurifère d'Omai est encaissé dans le Supergroupe Barama–Mazaruni, qui fait partie de la ceinture paléoprotérozoïque de roches vertes du Bouclier guyanais. Le gîte est relié principalement à un stock quartzomonzodioritique, le stock d'Omai, ainsi qu'à plusieurs filons tabulaires de porphyres quartzofeldspathiques et rhyolitiques et, en moindre volume, aux roches volcaniques et sédimentaires encaissantes. Dans le stock d'Omai, les veines montrent peu de variation de direction et pendage (généralement 030°/20°–30°), tandis que dans les filons de porphyres quartzofeldspathiques et rhyolitiques elles ont des directions et pendages aléatoires décrivant l'aspect typique en "stockwork". Les minéraux métalliques (moins de 2% du volume des veines) ont une minéralogie complexe qui consiste en plusieurs espèces de sulfures, associées à des éléments natifs, tellurures et sulfosels. Les tellurures comprennent principalement, en ordre d'abondance relative, tellurobismuthite, petzite, calaverite, hessite, altaïte, melonite, coloradoïte, and volynskite. L'assemblage métallique est defini par l'association Au–Ag–Te–W–Bi–Pb–Zn–Cu–Hg–Mo, qui est caractéristique à la fois des gisements épithermaux et mésothermaux. La gangue comprend principalement du quartz, avec des quantités mineures d'ankérite, calcite, muscovite, chlorite et épidote. Les conditions de la formation du gîte d'Omai ont été estimées à partir des données d'équilibre de l'assemblage des tellurures – sulfures – oxydes – silicates. La plupart des minéraux métalliques et de gangue ont été précipités à faible température (entre 220° et 170°C), à partir des solutions ayant des fugacités de faible variabilité en S_2 (de 10^{-17} à 10^{-11}), Te_2 (de 10^{-14} à $10^{-10.5}$) et O_2 (de 10^{-43} à 10^{-36}) et un pH faiblement acide (entre 4 et 5.4). L'or a probablement été transporté sous forme de complexes sulfurés [$Au(HS)_2^-$ et $Au(HS)^0$ ou $HAu(HS)_2^0$] ou thiosulfurés, tandis que le Te a été transporté comme H_2TeO_3, Te_2^{2-}, et HTe^-.

Mots-clés: gisement aurifère d'Omai, Bouclier guyanais, tellurures, fugacités de Te_2, S_2 et O_2, pH, analyses à la microsonde électronique.

§ *E-mail address*: gvoicu@sprint.ca

Introduction

The Omai gold deposit is the first producing gold mine in the Guiana Shield. It contains 120 tonnes of gold (past production plus reserves) occurring in quartz ± carbonate ± scheelite veins. The deposit is located in the Paleoproterozoic Barama–Mazaruni Supergroup of north-central Guyana (Fig. 1), a greenstone sequence consisting of mafic and felsic volcanic rocks and sedimentary rocks, intruded by granitic batholiths and stocks (Gibbs & Barron 1993). The gold-bearing veins occur within the epizonal Omai stock of quartz monzodioritic composition (Fennell pit), as well as within dikes of quartz–feldspar porphyry and rhyolite and, to a lesser extent, in surrounding andesite and basalt flows and metapelitic rocks (Wenot pit) (Voicu *et al.* 1997, Voicu 1999).

This study is specifically concerned with the telluride minerals and their relationship with coexisting sulfide and gangue minerals for each hydrothermal stage. These observations have been further used to establish the physicochemical characteristics of the environment of gold deposition. The telluride-bearing assemblages in conjunction with the thermodynamic data available for other mineral species provide narrower limits on conditions of deposition than the telluride-free assemblages. Knowledge of mineral assemblages and the physicochemical conditions of ore deposition at Omai can contribute to a better understanding of the Paleoproterozoic greenstone-hosted gold deposits in the Guiana Shield and West African Craton, where only a few such deposits, such as Ashanti, are well studied.

Background Information

The veins at Omai are undeformed and occupy extensional fractures between WNW–ESE-striking shear zones. The wallrocks and vein selvages commonly show discrete sheared planes, with both dextral and sinistral senses of movement. In the immediate vicinity of the quartz veins, the host rocks are altered to an assemblage of carbonate, quartz, white mica, chlorite, albite, pyrite and pyrrhotite. The hydrothermal assemblages are superimposed on an earlier phase of alteration related to spilitization of the volcanic rocks, and later greenschist-facies metamorphism.

In the Omai stock (Fennell pit), most veins are subparallel, thicknesses vary from a few cm up to about 1.5 m, and strike 025°–035°, with dips of 15–35° northwest. A subordinate set of veins strikes 300°–320° and dips 15°–35° southwest. The intersections of these two sets of veins are strongly enriched in gold. A third set, represented by thin (several cm thick) quartz veins, strikes *ca.* 330° and dips steeply (75°–85° in either direction). All sets of veins are contemporaneous, resulting in complex cross-cutting relationships.

In the Wenot pit, most mineralized veins are located in east–west-striking dikes of porphyry and rhyolite, and less commonly in andesites and metapelites. The veins have highly variable strikes and dips, which define typical stockwork mineralization. However, there are three principal sets of strikes and dips: 020°–040°/70°–85°, 020°–040°/30°–40°, and 090°–110°/70°–90°. The thickness of these veins is usually less than 0.3 m, whereas their frequency is significantly greater than in the Omai stock.

The gold-bearing veins appear to have formed by one or more episodes of fracturing and vein filling related to a protracted hydrothermal event. Two principal textures have been observed, namely "ribbon" and "breccia". Ribbons are defined by layers of minerals that may exceed 5 cm in thickness. The layers can be symmetrical about the median plane, indicating that opening of the veins took place on both walls of the vein, or asymmetrical, caused by reopening along one selvage. The core of the veins is generally occupied by quartz, but veins dominated by ankerite or scheelite, with minor quartz, occur locally in the Omai stock. Single- or multiple-stage brecciated veins contain angular or subrounded fragments of wallrocks reaching up to 0.8 m.

Telluride minerals were collected from the ribboned and breccia veins located in the Omai stock and in surrounding andesites and basalts. Tellurides were not observed in the gold-bearing veins from the Wenot pit.

Analytical Methods

Mineral compositions were determined on a JEOL electron microprobe at McGill University, at an accelerating voltage of 15 kV and a sample current of 20 nA on a Faraday cup. On-line ZAF corrections were performed with the MAGIC IV program. The following standards were used (in weight %): for Pd, Te and Hg, Pd_3HgTe_3 (synthetic), Pd 35.37, Hg 22.22, Te 42.41; for As, arsenopyrite, Fe 33.05, Co 0.58, Ni 0.21, As 45.61, Bi 0.88, S 19.67; for Bi, Bi_2S_3, Bi 81.29, S 18.71; for Pb, galena, Pb 86.60, S 13.40; for Fe, pyrite, Fe 46.55; S 53.45; for Au, Ag, Pt and Sb, pure metals. The composition of the standards was obtained by electron-microprobe analysis.

Vein Mineralogy

Table 1 summarizes the vein mineralogy for the three stages of mineralization at Omai. Ore minerals and gangue are represented by silicates (quartz, white mica, chlorite, epidote, albite), carbonates (ankerite, calcite), tungstates (scheelite), sulfides (pyrite, galena, chalcopyrite, pyrrhotite, sphalerite, molybdenite), oxides (hematite, magnetite, rutile), borosilicates (tourmaline), native elements (Au, Cu), tellurides, and sulfosalts. Table 2 lists the chemical composition of principal tellurides, sulfides, and native elements.

Quartz is the main vein-filling phase (65–98% of vein volume). Both smokey and milky quartz are related to mineralization. Scheelite and carbonate minerals occur as semicontinuous coatings along the vein selvages.

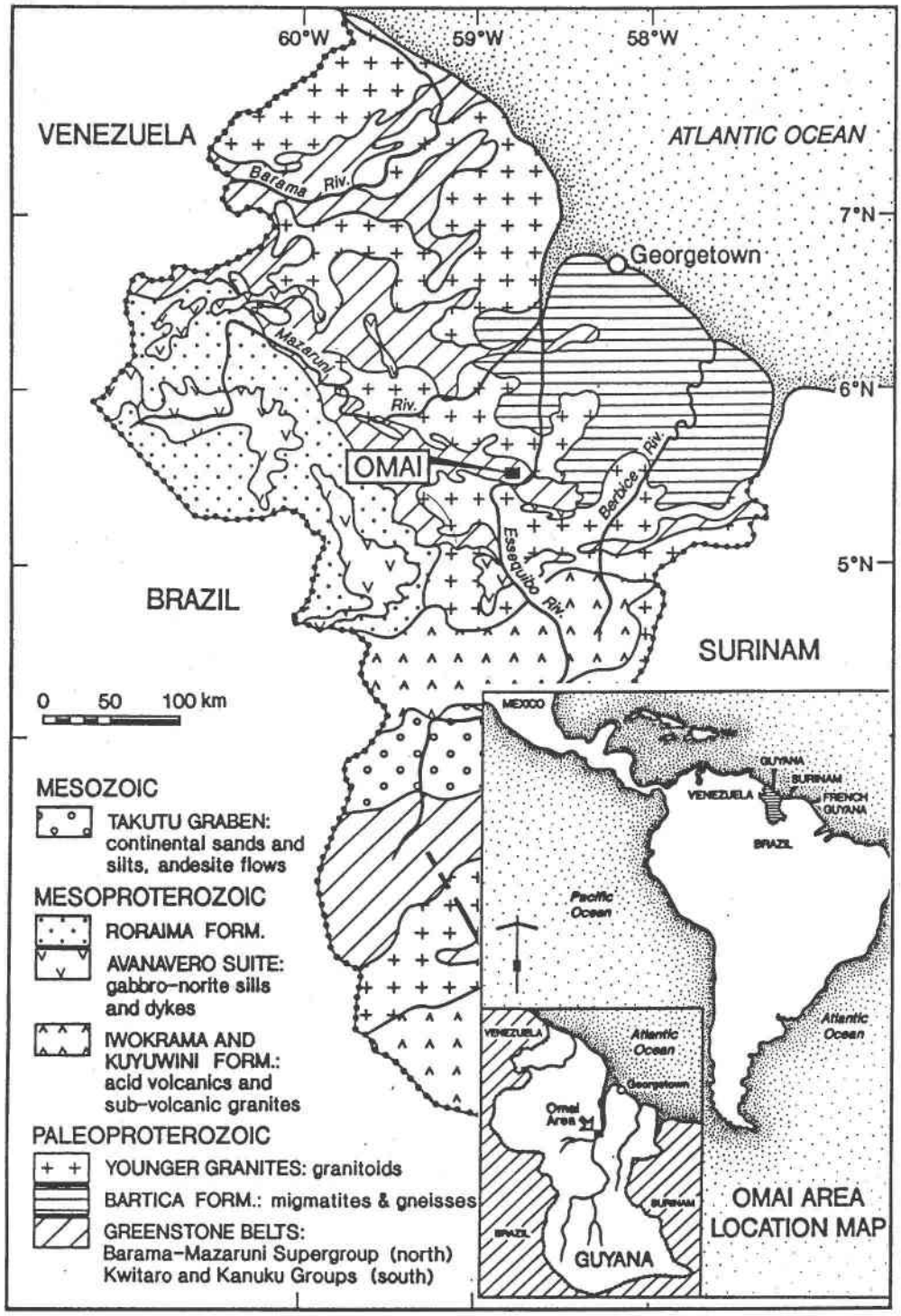

FIG. 1. Simplified geological map of Guyana, modified after Walrond (1987) and Gibbs & Barron (1993), showing location of the Omai mine.

TABLE 1. MINERAL ASSEMBLAGES IN THE MINERALIZED VEINS AT OMAI, GUYANA

STAGE I	STAGE II	STAGE III	POST-MIN*
smokey quartz, calcite, ankerite, chlorite, epidote, albite, scheelite, rutile, tourmaline, pyrite, magnetite, chalcopyrite, melonite, native gold	milky quartz, calcite, ankerite, white mica, pyrite, pyrrhotite, sphalerite, galena, chalcopyrite, hematite, calaverite, hessite, petzite, altaite, coloradoite, tellurobismuthite, native gold	milky quartz, calcite, white mica, pyrite, sphalerite, galena, chalcopyrite, molybdenite, calaverite, hessite, petzite, tellurobismuthite, native copper, native gold	translucent quartz, calcite

* Post-min: post-mineralization stage.

Gold appears relatively early in the ore paragenesis, although main-stage gold mineralization is associated with sulfide and telluride deposition during stages II and III. Free gold occurs as macroscopic irregularly shaped grains (up to 4 mm in diameter) or as dendritic fracture-filling in milky quartz, scheelite, and carbonates. Refractory gold occurs as small globular inclusions in pyrite (Fig. 2A) and pyrrhotite, usually in symplectitic intergrowths with sulfide and telluride minerals (Figs. 2B, C, G). The gold has a high fineness (950–990), and electrum has not been detected.

Pyrite is widespread at Omai and is characterized by brittle deformation, typically shown by fractured grains. The size of the pyrite grains ranges between a few mm and up to 5 cm. The pyrite grains are commonly veined and infilled along fractures and grain boundaries by a later generation of gold, telluride and sulfide minerals.

Pyrrhotite invariably occurs as pseudomorphs after pyrite. Perfect cubes of pyrrhotite, formed by partial or total replacement of pyrite, are observed in milky quartz and in wallrocks. Pyrrhotite pseudomorphs represent a significant site of deposition for gold, either as coatings on the grain boundaries or as fillings of fractures.

Other silicate, sulfide, oxide, and borosilicate minerals (see Table 1) represent minor phases, and occur locally.

Telluride Minerals

Telluride minerals are present as complex aggregates in ribbon- and breccia-textured quartz veins in the Omai stock. Telluride minerals occur randomly, in contrast with the zoned distribution described by Bowell *et al.* (1990) for the Paleoproterozoic tellurides at the Ashanti gold mine, Ghana. Three distinct generations of tellurides (I, II, and III) have been defined at Omai. The first generation is represented only by melonite ($NiTe_2$), which is associated with native gold, rutile and chalcopyrite in altered basalts, although its paragenetic position is not very well defined. Second-generation tellurides occur as small inclusions in pyrite II, whereas third-generation tellurides occur as a replacement of pyrite along healed fractures and as thin (1–2 mm) fracture-filling veinlets in quartz, carbonates and scheelite. All generations of telluride are associated with gold. Second- and third-generation telluride mineralogy is the same, except that coloradoite (HgTe) and altaite (PbTe) are found only in the second generation.

Au and Ag tellurides are represented by petzite ($AuAg_3Te_2$), calaverite ($AuTe_2$), and hessite (Ag_2Te). The most common is petzite, which varies from anhedral grains (Figs. 2B, C, D, E, G, H) to prismatic crystals up to 2 mm in length. The sharp contacts between petzite and other Au–Ag tellurides and the complex textural relationships indicate their coeval precipitation from the ore fluid. However, in several samples, the association petzite–hessite has many characteristics similar to those described by Kelly & Goddard (1969), which suggest that they are the product of decomposition of the χ phase at 120°C (Cabri 1965, Afifi *et al.* 1988, Cooke *et al.* 1996). Therefore, two generations of petzite and hessite probably exist at Omai, the first as primary mineral phases and the second as low-temperature products of decomposition of the χ phase.

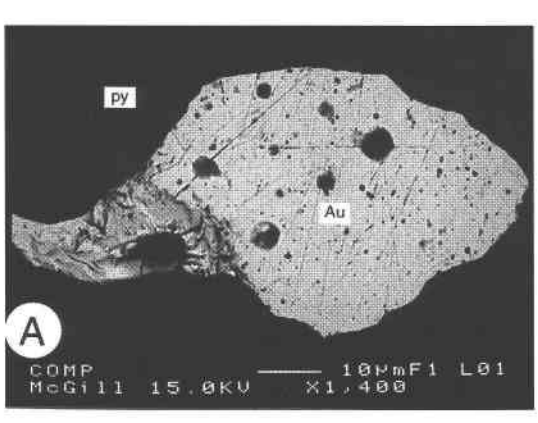

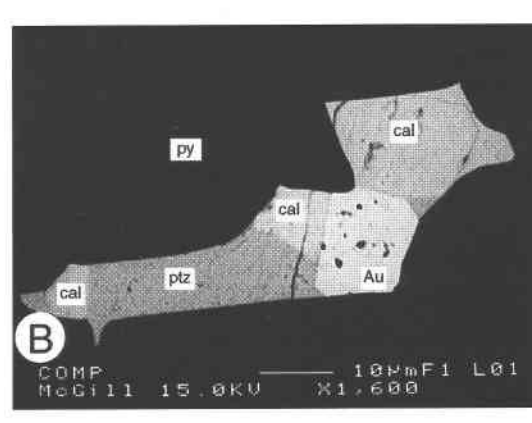

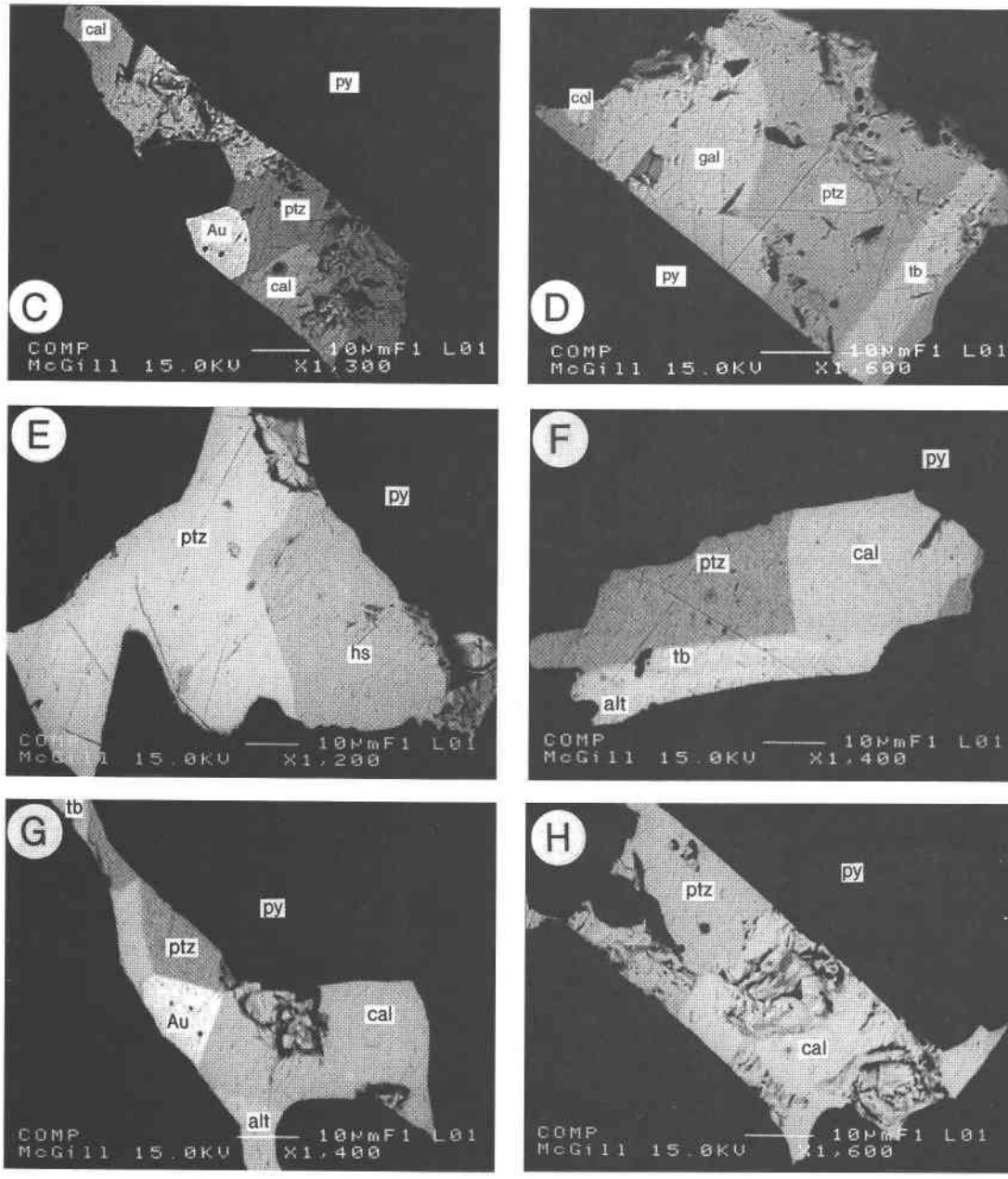

FIG. 2. Back-scattered electron images of polished sections of gold inclusions in pyrite (A) and of symplectitic intergrowths among tellurides, sulfides, and gold (B–H). Abbreviations: Au: native gold, alt: altaite, cal: calaverite, col: coloradoite, gal: galena, hs: hessite, py: pyrite, ptz: petzite, tb: tellurobismuthite. Scale bar: 10 μm.

TABLE 2. REPRESENTATIVE COMPOSITIONS* OF NATIVE ELEMENTS, TELLURIDES AND COMMON SULFIDES, OMAI, GUYANA

Mineral	Stage	Au	Ag	Pb	Bi	Fe	Pt	Ni	Zn	Te	S	Sb	Hg	Total
Native gold	Au I	92.80	5.40	0	0	0.62	0	0	0	0.01	0.07	0	n.a.	98.99
	Au I	90.44	8.71	0	0.11	1.91	0	n.a.	n.a.	0.08	0.31	0	1.11	102.67
	Au II	97.01	2.78	0	0	0.01	0	0	0	0	0.02	0	n.a.	99.82
	Au III	92.80	5.37	0	0	0.62	0	n.a.	n.a.	0.01	0.06	0	n.a.	98.89
	Au III	92.81	5.99	0	0	0.42	0	n.a.	n.a.	0.04	0.07	0	1.22	100.58
Petzite	Ptz II	24.01	42.10	0	0.05	0.44	0.01	0	0	32.43	0.10	0.16	n.a.	99.39
$AuAg_3Te_2$	Ptz II	20.82	46.37	0	0	0.58	0	n.a.	n.a.	32.52	0.09	0.17	0.14	100.35
	Ptz II	22.33	43.54	0	0	0.91	0	n.a.	n.a.	32.09	0.15	0.16	0.10	99.31
	Ptz II	24.45	44.14	0	0	0.17	0.01	0	0	30.17	0.10	0.16	n.a.	99.22
	Ptz III	25.30	45.64	0	0	0.07	0	0	0	29.94	0.10	0.15	n.a.	101.21
Calaverite	Clv II	41.68	0.71	0	0.19	0.35	0	n.a.	n.a.	54.41	0.01	0.36	0.58	98.38
$AuTe_2$	Clv II	41.69	0.75	0	0.07	0.76	0	n.a.	n.a.	54.27	0.02	0.32	0.45	98.39
	Clv II	41.55	0.04	0	0.16	0.80	0	0	0	55.09	0.04	0.31	n.a.	98.08
Hessite	Hes II	0.68	60.48	0.07	0	0.19	0	0	0	37.17	0.09	0.18	n.a.	98.82
Ag_2Te	Hes II	0.67	59.13	0	0	0.33	0	0	0	37.38	0.09	0.22	n.a.	97.78
Telluro-	Tbm II	0	0	0	53.15	0.32	0.01	0	0	44.79	0.28	0.28	n.a.	98.86
bismuthite	Tbm III	0	0	0.04	51.76	0.14	0	0	0	45.25	0.05	0.23	n.a.	97.56
Bi_2Te_3	Tbm III	0	0	0	51.58	0.37	0	0	0	45.78	0.01	0.33	n.a.	98.10
Melonite		0	0	0	0.01	0.80	0	20.82	0	79.18	0.23	0	n.a.	101.04
$NiTe_2$		0	0.05	0	0.16	5.88	0	15.38	0	69.82	8.24	0.47	0	100.06
Altaite		0.00	0.16	57.25	0.15	0.59	0.01	n.a.	n.a.	35.60	0.05	0.24	n.a.	94.06
PbTe		0.04	0.08	58.14	0.10	1.24	0.05	n.a.	n.a.	35.52	0.38	0.22	n.a.	95.78
Coloradoite (Hg,Ag)Te		0.04	13.34	0	0	1.54	0.08	n.a.	n.a.	34.75	0.25	0.17	51.41	101.15
Galena	Gn III	0.01	0	83.93	0	0.10	0.08	n.a.	n.a.	0.15	12.92	0	n.a.	97.27
	Gn III	0	0	83.59	0	0.19	0.01	n.a.	n.a.	0.06	13.11	0	n.a.	96.94
	Gn II	0.00	0	86.57	0	0.52	0.00	n.a.	n.a.	0.03	13.20	0	n.a.	100.42
Sphalerite	Sp II	0.00	0	0	0	1.59	0	n.a.	67.04	0	30.70	n.a.	n.a.	99.33
Pyrite	Py III	n.a.	n.a.	n.a.	n.a.	51.35	n.a.	n.a.	0	n.a.	48.63	n.a.	n.a.	99.96
		n.a.	n.a.	n.a.	n.a.	51.29	n.a.	n.a.	0	n.a.	49.07	n.a.	n.a.	100.32
Pyrrhotite		0	n.a.	n.a.	n.a.	62.67	n.a.	1.43	0	n.a.	34.32	n.a.	n.a.	98.40
		0	n.a.	n.a.	n.a.	61.20	n.a.	n.a.	n.a.	n.a.	36.53	n.a.	n.a.	97.72

n.a.: not analyzed; 0: below detection limit. * The compositions are expressed in weight %. Symbols: Clv calaverite, Gn galena, Hes hessite, Ptz petzite, Sp sphalerite, Tbm tellurobismuthite.

Calaverite coexists with primary hessite (Fig. 3), which suggests that these two minerals may form at similar $f(O_2)$–pH conditions at temperatures less than about 300°C (Legendre *et al.* 1980, Jaireth 1991, Zhang & Spry 1994). Their association is in contradiction with the predicted occurrence in nature of the calaverite–γ phase ($Ag_{1.89–1.97}Te$; Cabri 1965, Pohl & Beaty 1990).

Tellurobismuthite (Bi_2Te_3) represents the most common telluride at Omai (Figs. 2D, F). It is commonly associated with native gold, petzite, altaite and galena. At Omai, Bertoni *et al.* (1991a, b) also identified native bismuth, tetradymite (Bi_2Te_2S), and "wehrlite" (originally described as BiTe; Brown & Lewis 1962). Elliott (1992) also reported "wehrlite" at Omai, although its chemical composition is similar to that of pilsenite (Bi_4Te_3), in agreement with the fact that "wehrlite" actually represents a mixture of pilsenite and hessite (Ozawa & Shimazaki 1982, Dobbe 1993). However, it is of interest to note a gradual variation of the Te/Bi, Te/S and Bi/S values, which resulted in the precipita-

tion of various Bi-bearing tellurides ± sulfosalts. The substitution of Sb for Bi, up to 0.08 wt% in tellurobismuthite, is probably due to the isostructural nature of Bi_2Te_3 and Sb_2Te_3 (tellurantimony). The absence of native tellurium, correlated with the presence of native Bi and Bi-rich mineral phases, suggests that the Omai assemblage lies on the Bi-rich side of the single Bi–Te solid-solution phase (Dobbe 1993). These assemblages characterize telluride-undersaturated fluids (*cf.* Ahmad *et al.* 1987, Afifi *et al.* 1988, Zhang & Spry 1994) at a neutral to acid pH and a redox state near the magnetite–hematite buffer (*cf.* McPhail 1995).

Altaite (PbTe) and Ag-bearing coloradoite [(Hg,Ag)Te ?] are minor phases that occur in association with galena and tellurobismuthite (Figs. 2D, F, G), and probably formed by contemporaneous crystallization from Pb–Bi–Hg–Te-rich fluids. However, as galena can incorporate appreciable levels of Te and Hg in its structure (>100 ppm Te, Dobbe 1993; >300 ppm Hg, Schalamuk & Logan 1994), the segregation of native bismuth and Hg–Te minerals and the replacement of galena by altaite cannot be disregarded. As the analyzed coloradoite is very small and in contact with a grain of petzite, it is possible that part of the Ag content detected in coloradoite belongs to petzite.

Melonite ($NiTe_2$) is very rare at Omai. Usually, melonite is associated with magmatic copper–nickel deposits related to mafic and ultramafic rocks (*e.g.,* Rao *et al.* 1980, Hudson 1986, Garuti & Rinaldi 1986), Phanerozoic epithermal veins (*e.g.,* Shimada *et al.* 1981, Ahmad *et al.* 1987, Afifi *et al.* 1988), and epithermal to mesothermal quartz veins of several Precambrian greenstone terranes (*e.g.,* Harris *et al.* 1983, Tremlow 1984, Phillips 1986, Robert & Brown 1986, Milési *et al.* 1992). At Omai, melonite is disseminated in weakly carbonate-altered basalts, associated with gold, chalcopyrite, and rutile (formed from ilmenite) (Fig. 4). However, it is difficult to assess if melonite has a genetic relationship with the pervasive ankerite alteration or if it represents a mineral phase crystallized from a relatively Te-enriched basic to intermediate melt, that underwent subsequent subsolidus modification. Taking into consideration the general enrichment of Ti in the hydrothermal fluids at Omai and the low concentrations of Te in the host rocks (Voicu *et al.* 1997), we favor a genetic relationship between melonite and the Te-bearing mineralizing fluids.

Johnston (1960), Bertoni *et al.* (1991b), and Elliott (1992) noted several tellurides and sulfosalts at Omai that were not been encountered in our study. These are volynskite ($AgBi_{1.6}Te_2$), nagyágite [$Pb_5Au(Te,Sb)_4S_{5-8}$], and aikinite ($PbCuBiS_3$). Volynskite was determined by electron microscopy (Elliott 1992) and has a similar chemical composition to volynskite from the Yokozuru (Japan) and Ashley (Ontario) gold deposits (Shimada *et al.* 1981, Harris *et al.* 1983). For nagyágite and aikinite, identified only by optical methods, their presence remains equivocal.

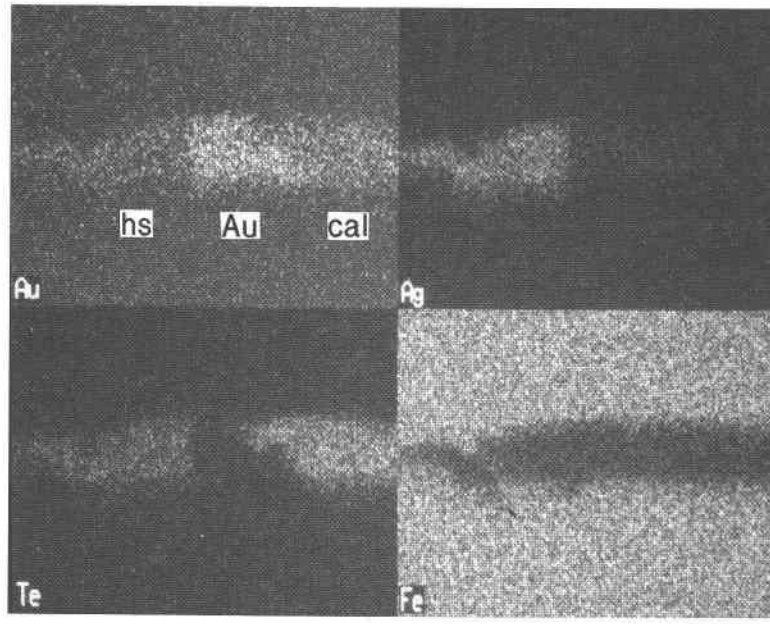

FIG. 3. Single-element scanning electron micrograph for Au, Ag, Te, and Fe of the gold – calaverite – hessite association in pyrite. Abbreviations are the same as in Figure 2.

Physicochemical Conditions of Ore Formation

Minerals in the system Au–Ag–Te commonly form in the last stages of epithermal and mesothermal gold–silver systems (*e.g.*, Robert & Brown 1986, Bowell *et al.* 1990, Zhang & Spry 1994). Thermodynamic data for this system are available for only a few species (calaverite, hessite, native gold, silver and tellurium), which does not allow the calculation of complete physicochemical conditions of ore formation. In contrast, the telluride-bearing assemblages, in conjunction with the thermodynamic data available for other mineral species (sulfides, oxides, carbonates, silicates), may provide narrower limits on conditions of deposition than the telluride-free assemblages, and may place tighter constraints on the physicochemical conditions of the ore-forming fluids.

The conditions of ore formation at Omai can be estimated from the stability of telluride – sulfide – oxide – silicate minerals of each hydrothermal stage. Because all variables considered [$f(Te_2)$, $f(O_2)$, $f(S_2)$, temperature, and pH] cannot be represented simultaneously on one diagram, we have considered temperature as the principal factor that influences and relates all other variables. The temperature data have been obtained using stable isotope geothermometers and the Na–K–Ca geothermometer of Fournier & Truesdell (1973), based on cation proportions established from fluid inclusions in silicates, scheelite, carbonates, sulfides, and native gold by means of the crush–leach technique and capillary electrophoresis (Hallbauer 1994, Hallbauer & Voicu 1998). A summary of the temperature values of the vein-forming minerals is presented in Table 3. The three main hydrothermal stages are considered to have

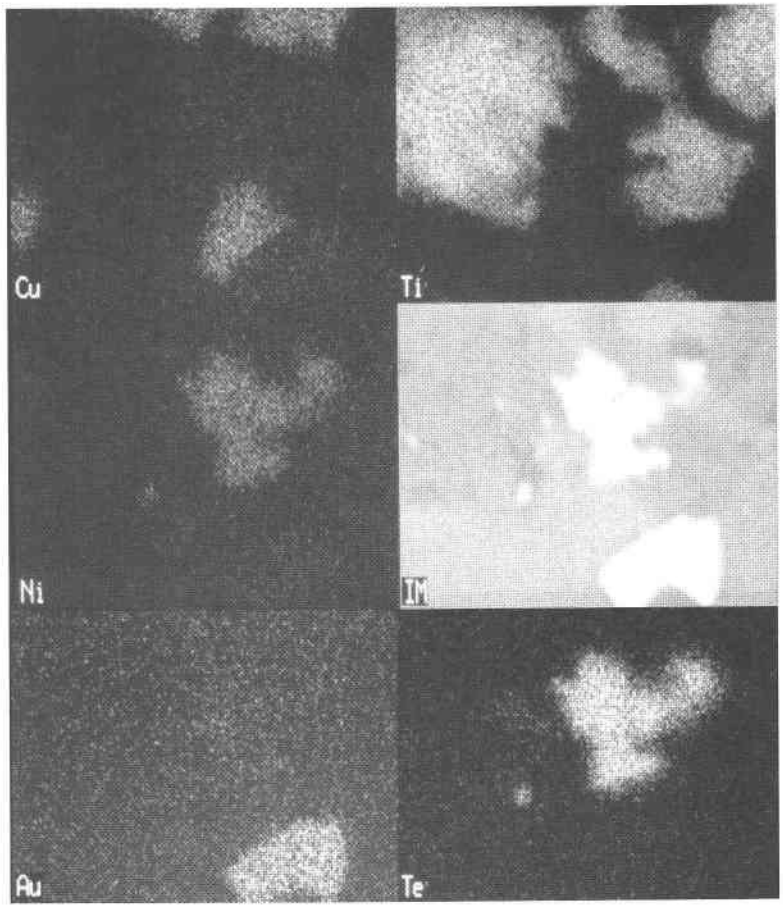

Fig. 4. Single-element scanning electron micrograph for Au, Te, Cu, Ti, Ni and the analyzed area of the melonite – native gold – chalcopyrite – rutile assemblage. The rutile is formed from ilmenite.

TABLE 3. TEMPERATURE (°C) OF FORMATION OF THE VEIN-FORMING MINERALS AT OMAI, GUYANA

Mineral	Stage I	Stage II	Stage III
Scheelite	$257 \pm 8^{(1)}$, $n = 7$ $180 \pm 45^{(2)}$, $n = 7$		
Quartz	$257 \pm 8^{(1)}$, $n = 7$ $175 \pm 22^{(2)}$, $n = 6$ 215–300[3]	$168 \pm 20^{(2)}$, $n = 13$ 195–205[3]	170–185 [3]
Epidote	$225 \pm 11^{(2)}$, $n = 4$		
Ankerite		$195 \pm 7^{(1)}$, $n = 6$ $178 \pm 5^{(2)}$, $n = 4$	
Calcite		$198 \pm 10^{(1)}$, $n = 5$ $190 \pm 13^{(2)}$, $n = 3$	
Albite	$213^{(2)}$, $n = 1$		
Pyrite	$243 \pm 8^{(2)}$, $n = 3$	$197 \pm 19^{(2)}$, $n = 2$	
Galena			$177^{(2)}$, $n = 1$
Chalcopyrite		$201 \pm 2^{(2)}$, $n = 2$	
Native gold		$198^{(2)}$, $n = 1$	$166^{(2)}$, $n = 1$
Average T (°C)	225 ± 25	192 ± 8	172 ± 5

n: number of samples; standard errors quoted as 2σ. (1) Isotopic temperatures calculated by combining oxygen isotope fractionation equations between scheelite and H_2O (Wesolowski & Ohmoto 1986), quartz and H_2O (Clayton *et al.* 1972), and calcite and H_2O (O'Neil *et al.* 1969). (2) Temperature calculated using Na–K–Ca geothermometer of Fournier & Truesdell (1973). The data are taken from Hallbauer & Voicu (1998), and Voicu (1999). (3) Temperature of homogenization of the primary fluid inclusions (Elliott 1992).

formed in the order at 220°, 200°, and 170°C. For stage I, an average temperature of 220°C was used, owing to discrepancies in temperature values for quartz and scheelite between isotopic and cation-based geothermometers. Therefore, it is possible that the average temperature for this stage exceeds 220°C. In order to better constrain the physicochemical conditions of mineral deposition, the following discussion considers each hydrothermal stage as a separate mineralizing event. However, the Omai deposit probably represents the result of a continuous hydrothermal process, each stage of fluid activity being characterized by gradual physical and chemical changes. This interpretation is supported by the sequential deposition of several mineral phases (quartz, carbonates, white mica, gold, pyrite, chalcopyrite, galena, tellurides) and by the overlap in range of $f(S_2)$, $f(Te_2)$, $f(O_2)$, and pH of the hydrothermal fluids (see below).

Tellurium and Sulfur Fugacities

The mineral paragenesis observed for each stage of mineralization, superimposed on experimental data in the systems Au–Ag–Te, Cu–Fe–S–O and Bi–Pb–Hg–Ni–Te–S (Barton & Skinner 1979, Afifi *et al.* 1988, Zhang & Spry 1994), allows an estimate to be made of the variation in Te_2 and S_2 fugacities. Because there are no significant changes to the location of stability fields at temperature as high as 220°C, and as low as 170°C, an average temperature of 200°C was chosen. The main characteristics of each hydrothermal stage follow (Fig. 5):

Stage I: Coexisting pyrite and magnetite suggest that early sulfides were deposited at conditions between the stabilities of the reactions: pyrrhotite + S_2 = pyrite + magnetite and magnetite + S_2 = hematite + pyrite. The presence of melonite indicates that the $f(Te_2)$ at a given $f(S_2)$ was above the hessite–acanthite reaction, which defines the minimum $f(Te_2)$ for the stability of tellurides. The absence of Au–Ag–Pb–Bi tellurides and sulfides is thus due to the absence of these elements in the hydrothermal fluids during this mineralizing stage, rather than to the physicochemical conditions of deposition. The presence of melonite and absence of millerite indicate that $f(Te_2)$ were above the millerite–melonite reaction. A $f(S_2) - f(Te_2)$ diagram at an average temperature of 200°C shows a variation range of $\log f(S_2)$ between –14 and –17, and a $\log f(Te_2)$ value higher than –14 (Fig. 5).

Stage II: The presence of coloradoite instead of cinnabar or native Hg indicates that fugacities were above the coloradoite–cinnabar and coloradoite – native Hg reactions. The complex association of Bi tellurides and sulfides suggests a gradual change in the ratio $f(Te_2)/f(S_2)$, which probably initially increased compared to stage I, allowing the gradual formation of pyrrhotite, galena and altaite, followed by an increase of $f(Te_2)$ and $f(S_2)$ forming tellurobismuthite, pilsenite (and possibly hessite), and galena. This behavior explains the abundance of galena compared to other Bi–Pb tellurides and sulfides. A further increase of the $f(Te_2)$ resulted in the deposition of petzite, hessite and calaverite. The presence of hematite + pyrite indicates that $f(S_2)$ was on the high-$f(S_2)$ side of the reaction magnetite + S_2 = hematite + pyrite. The sulfur fugacity can be determined for this stage from the FeS content of sphalerite coexisting with pyrite. The sphalerite from Omai generally contains less than 2 mole % FeS. Using an average value of 1 mole % FeS in sphalerite, a temperature of 200°C, and the equation of Barton & Skinner (1979), one obtains

$$\text{Log } X_{Fe(Sphalerite)} = 7.16 - 7730/T - 1/2 \log f(S_2) \quad (1)$$

where T is in Kelvin, the calculated $\log f(S_2)$ is –18.3. However, the presence of ditellurides and of hematite–magnetite and galena–altaite assemblages indicates that the terminal part of this stage is characterized by an increase of $\log f(S_2)$ up to ~–13.5, associated with an increase of $\log f(Te_2)$. The upper and lower limits of $f(Te_2)$ can be defined by the absence of stützite [$\log f(Te_2) < -10.5$] and the presence of calaverite [$\log f(Te_2) > -11.2$].

Stage III: The predominance of sulfide over tellurium minerals indicates lower Te_2/S_2 values in the hydrothermal fluids compared to the previous stage. This

is probably due to the increase of $f(S_2)$ rather than the decrease of $f(Te_2)$, as suggested by the continued presence of ditellurides such as calaverite at this hydrothermal stage. Therefore, the $\log f(Te_2)$ probably varies over the same range as for stage II (between –11.2 and –10.5). The limits of $f(S_2)$ variation are constrained by the absence of magnetite and altaite, and the presence of chalcopyrite instead of bornite. The $\log f(S_2)$ during this stage varied between –13.5 and –11. As in the previous stage, the mineral assemblages show that the mineralizing fluids were saturated with tellurides, but undersaturated with respect to native tellurium. As the mineral deposition of this stage took place at lower temperatures, the cooling paths of the fluids were associated with an almost constant fugacity of tellurium.

Oxygen fugacities and pH

The $f(O_2)$–pH values of the mineralizing fluids can be constrained for stages II and III. The salinity data used here are based on a fluid-inclusion study by Elliott (1992). A representative salinity of the hydrothermal fluids is taken to be 1 wt% NaCl, which corresponds to a concentration of 0.08 *m* Na^+ and an ionic strength (I) of 0.4. Assuming that Na/K was 1:1, the K^+ concentration was 0.08 *m*. The calculated concentrations were converted to activities ($\log aNa^+ = \log aK^+ = -1.4$) using the extension of the Debye–Hückel equation (Helgeson 1969, Cooke *et al.* 1996) in order to calculate fields of potassium-bearing minerals as a function of pH. Total dissolved gold (ΣAu), silver (ΣAg) and tellurium (ΣTe) = 1 ppb have been assumed and represent the common amount for hydrothermal fluids that form at low temperature (Zhang & Spry 1994, McPhail 1995).

Using a temperature of 200°C and the mutual stability of the hessite – calaverite – pyrite – chalcopyrite – white mica assemblage during stage II, the values obtained for $\log f(O_2)$ vary between –36 and –38, whereas the values of pH range between 4.2 and 5.4 (Fig. 6). The oxidation condition is above the hematite–magnetite buffer, but below the necessary conditions for hematite saturation. Stage III is characterized by a similar assemblage of minerals, but a lower temperature (170°C) than stage II. Using a similar composition of the fluid as for stage II, the $\log f(O_2)$ value ranged between –39 and –43, and pH ranged between 4 and 5.2.

The pH range between 4 and 5.4 for stages II and III is grossly similar to that of the typical greenschist-facies mesothermal gold deposits (pH ≈ 5.2 to 6.2) and to that of shallow-level Archean gold deposits (pH between 4.1 and 5.2) at an equivalent temperature (~200°C) (Gebre-Mariam *et al.* 1993, Hagemann *et al.* 1994).

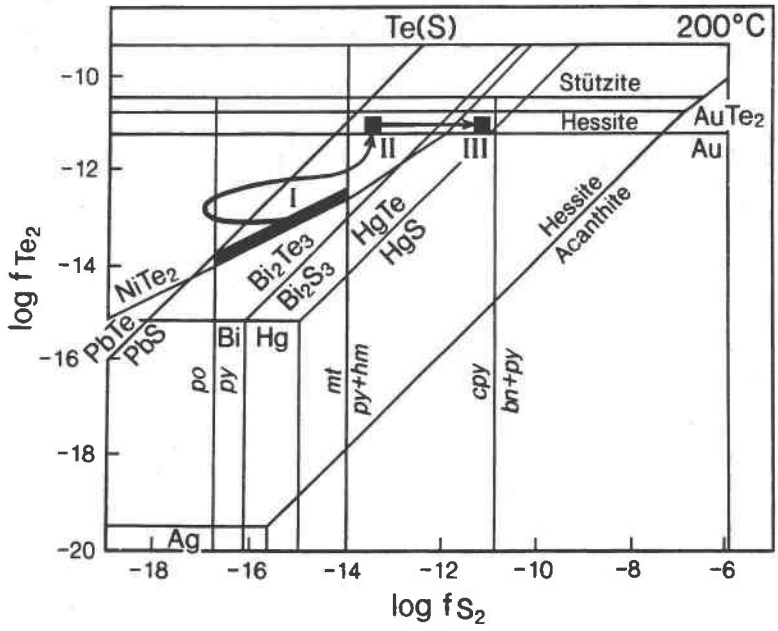

FIG. 5. Variations of Te_2 and S_2 fugacities with respect to selected telluride–sulfide assemblages at a temperature of 200°C (modified after Afifi *et al.* 1988). Hessite–γ phase reaction was modified in order to accommodate the calaverite – hessite assemblage observed at Omai. Arrows show fugacity variations during the hydrothermal stages (I, II, and III) of the Omai gold deposit. Abbreviations: bn: bornite, hm: hematite, mt: magnetite, py: pyrite, po: pyrrhotite.

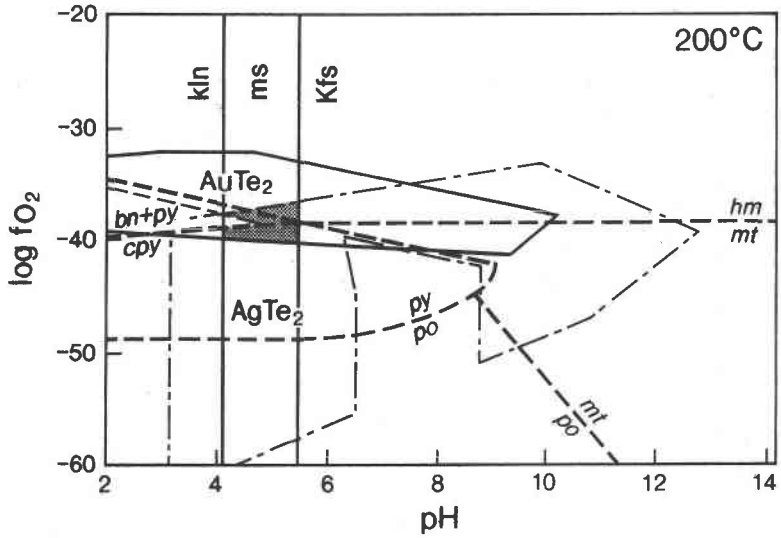

FIG. 6. Diagram showing the fugacity of oxygen *versus* pH and the environment of deposition at Omai in stage II. The stability boundaries of calaverite (solid lines) and hessite (dashed – single dotted lines) (data from Zhang & Spry 1994) are superimposed onto the systems Fe–S–O, Cu–Fe–S, and K–Al–Si–O–H (calculated using SUPCRT software, Johnson *et al.* 1992) for the following conditions: T = 200°C, I = 0.4, ΣS = 0.01 *m*, ΣAu = 1 ppb, ΣAg = 1 ppb, ΣTe = 1 ppb, K^+ = 0.08 *m* (see text for discussion of estimates of concentration). Abbreviations: kln: kaolinite, ms: white mica, Kfs: potassium feldspar. The other abbreviations are the same as in Figure 5.

METAL TRANSPORT

Gold is usually transported either as chloride or sulfide species. The physicochemical conditions at Omai (temperatures less than 220°C, low salinity, low pressure, weakly acid pH) suggest that the major Au-bearing species are most likely to have been $Au(HS)^{2-}$ and $Au(HS)^0$ or $HAu(HS)_2^0$ (*cf.* Seward 1991, Hayashi & Ohmoto 1991, Benning & Seward 1994, Ridley *et al.* 1996, Cooke *et al.* 1996). The stability field for $Au(HS)^{2-}$ is largely coincident with the stability field for pyrite, indicating that gold may be transported and deposited in equilibrium with pyrite (Shenberger & Barnes 1989). $Au(HS)^0$ and $HAu(HS)_2^0$ complexes are important where gold is precipitated in equilibrium with white mica from weakly acidic to neutral conditions (pH ≤ 5.5), as at Omai. On the other hand, the analysis of fluid inclusions in sulfides (pyrite, chalcopyrite, and galena) and native gold from Omai by capillary electrophoresis detected significant quantities (up to 1130 ppm) of the thiosulfate ($S_2O_3^{2-}$) complex (Hallbauer & Voicu 1998, Voicu 1999). However, it is difficult to distinguish primary $S_2O_3^{2-}$ and that produced by post-entrapment of the inclusion fluid owing to diffusive loss of H_2. As suggested by Kucha *et al.* (1994), assemblages that contain pyrite and complexes with an intermediate valence of sulfur may be a product of fluids bearing polysulfide – thiosulfate – sulfide. These fluids form by the interaction between deep higher-temperature fluids and oxygenated, near-surface groundwaters (Groves & Foster 1991, Kucha *et al.* 1994). They are very efficient at transporting gold at temperatures of around 200°C and may account for the association of gold and thiosulfate complexes identified at Omai.

Telluride minerals are volumetrically minor at Omai, but their presence is useful in unravelling the reasons for deposition. The following parameters have been used: equilibrium constants for reactions at 200°C, $f(O_2)$ between –36 and –38, and 4.2 < pH < 5.4 (for stage II), $f(O_2)$ between –39 and –43, and 4 < pH < 5.2 (for stage III), in the system Au–Ag–Cl–S–O–H (Zhang & Spry 1994), superimposed onto the systems Te–O–H (McPhail 1995, Cooke *et al.* 1996) and Fe–S–O (Barton & Skinner 1979) (Fig. 7). The predominant aqueous species of tellurium are calculated to be H_2TeO_3 (for stage II) and H_2TeO_3, Te_2^{2-} and HTe^- (for stage III). These aqueous species of tellurium occur under oxidizing conditions in stage II (higher than the hematite–magnetite buffer), whereas for stage III there is a gradual transition from oxidizing to more reducing conditions. The most important aqueous gold–silver-bearing species responsible for the formation of gold–silver telluride minerals are $Au(HS)^0$ or HAu(HS) and $Ag(HS)^0$ or $HAg(HS)_2^0$. We have not considered thiosulfate com-

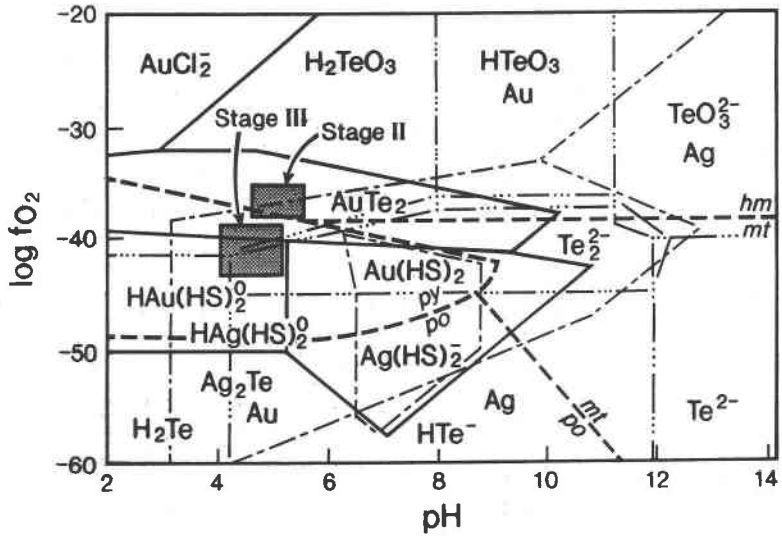

FIG. 7. Diagram showing log $f(O_2)$ *versus* pH for the system Te–O–H (dashed – triple dotted lines), superimposed onto the systems Au–Te–Cl–S–O–H (solid lines), Ag–Te–Cl–S–O–H (dashed – single dotted lines), and Fe–O–S (dashed lines) at the following conditions: T = 200°C, ΣS = 0.01 *m*, ΣAu = 1 ppb, ΣAg = 1 ppb, m_{Cl^-} = 0.1. Contours of the predominance of Te_2^{2-} are drawn at log $f(Te_2)$ = –11. Thermodynamic data are from Barton & Skinner (1979), Zhang & Spry (1994), McPhail (1995), and Cooke *et al.* (1996). The dark solid rectangles represent the estimated composition of the hydrothermal fluids (stages II and III) responsible for the mineralization at Omai. Abbreviations are the same as in Figure 6.

plexes. $Au(HS)^{2-}$, $Ag(HS)^{2-}$ and chloride species seem to have played a minor role, at best, in the transport and deposition of gold–silver tellurides in the temperature, pH, and $f(O_2)$ range of the Omai deposit.

Discussion and Conclusions

The calaverite–hessite association should be interpreted to mean either that there is a non-equilibrium assemblage at Omai or that the γ phase cannot exist in nature, and the hessite – γ phase reaction is above the native gold – calaverite transition and very close to the γ phase – stützite ($Ag_{5-x}Te_3$) reaction (at higher Te fugacity). Calaverite and hessite at Omai are not in mutual contact. A grain of gold separates them from one another (Fig. 3), and it is unclear whether they were deposited together. Harris (1989) provided a similar example for the Hemlo deposit, Ontario, where the assemblage calaverite – hessite – gold coexists in the same hand sample. Zhang & Spry (1994) left open the question regarding the stability of calaverite + hessite, whereas Legendre *et al.* (1980) inferred that these minerals form a stable assemblage between 140° and 310°C. In the latter situation, a stable calaverite–hessite assemblage strongly decreases the Te stability field of the γ phase. Formation of the γ phase becomes restricted to a very narrow range of variation of $f(Te_2)$ between hessite + calaverite and stützite fields, which drastically diminishes the chances of finding it in natural assemblages. The calaverite–hessite association has been also described by Cooke *et al.* (1996) at Acupan, Philippines, Bowell *et al.* (1990) at Ashanti, Ahmad *et al.* (1987) at Emperor, Fiji, Siddeley & Araneda (1986) at El Indio, Chile, and Thompson *et al.* (1985) at Cripple Creek, Colorado. Because the presence of the γ phase, similar in chemical composition to hessite ($Ag_{1.95-1.97}Te$), was claimed only by Pohl & Beaty (1990), we postulate a direct hessite–stützite reaction in natural samples. The synthetic γ phase is thus considered to be a metastable intermediate phase within a very narrow range of temperature and Te fugacity between hessite and stützite. This interpretation can only be verified once thermodynamic data for stützite become available.

The mineral assemblage represented by various sulfides and tellurides can be used to constrain the chemical conditions of ore transport and deposition. The physicochemical parameters of the Omai hydrothermal system can be summarized as follows:

1) Gradual, but limited cooling of the mineralizing fluids, characterized by mesothermal temperatures dur-

ing the early stage, was followed by temperature intervals that are similar to those of the epithermal deposits.

2) Variable $f(S_2)/f(Te_2)$ values of each hydrothermal stage allowed the deposition of various sulfide and telluride minerals. The solutions were Te-undersaturated, allowing ditelluride deposition, while inhibiting the formation of native tellurium and stützite. The formation of Ag – Te ± Au mineral phases instead of Ag–Au alloy was greatly influenced by the Te concentration of the hydrothermal fluids. An increase of sulfur fugacity at an almost constant tellurium fugacity during the last stages of mineralization allowed complete deposition of sulfides, tellurides, and gold. Post-mineralization fluids were barren of metals.

3) Conditions of pH showed constant values (between 4 and 5.4) for both main mineralizing stages of mineralization. A gradual transition from oxidizing conditions to a reducing environment could be the result of fluid–rock interaction associated with strong sulfidation of the wallrock.

4) Sulfides were probably transported as sulfide or thiosulfate complexes, whereas Te was transported as aqueous H_2TeO_3, Te_2^{2-}, and HTe^- complexes.

Acknowledgements

Supporting funds from Omai Gold Mines Ltd., Cambior Inc. and Golden Star Resources to GV and MB and a Natural Sciences and Engineering Research Council of Canada scholarship to GV are gratefully acknowledged. We thank D.K. Hallbauer for permission to quote unpublished data on fluid composition and temperature. The manuscript has benefitted greatly from the critical comments of E.T.C. Spooner, K. M. Ansdell, F. Robert, R.R. Seal, D.J. Kontak, R.F. Martin and an anonymous reviewer. We also thank R. Crépeau and F. Viens (Cambior) and C. Bertoni (Golden Star Resources) for making this study possible, Y. Michaud, C. Poulin, B. Westin, E. Belzile, and B.J. Bhatt (Omai Gold Mines, Cambior Inc.) for their cooperation, R. Mineau (UQAM) for scanning electron microscopy, G. Poirier (McGill University) for electron-microprobe analyses, M. Preda (UQAM) for X-ray-diffraction analyses, G. Robert for polished and thin sections, and M. Laithier for drafting most figures.

References

Afifi, A.M., Kelly, W.C. & Essene, E.J. (1988): Phase relations among tellurides, sulfides, and oxides. II. Applications to telluride-bearing ore deposits. *Econ. Geol.* **83**, 395-404.

Ahmad, M., Solomon, M. & Walshe, J.L. (1987): Mineralogical and geochemical studies of the Emperor gold telluride deposit, Fiji. *Econ. Geol.* **82**, 345-370.

Barton, P.B., Jr. & Skinner, B.J. (1979): Sulfide mineral stabilities. *In* Geochemistry of Hydrothermal Ore Deposits (H.L. Barnes, ed.; second edition). Wiley Interscience, New York, N.Y. (278-403).

Benning, L.G. & Seward, T.M. (1994): Hydrosulphide complexes of gold(I) at high pressures and temperatures: equilibrium and kinetic problems. *Mineral. Mag.* **58A**, 75-76 (abstr.).

Bertoni, C.H., Shaw, R.P., Singh, R., Belzile, E., Minamoto, J., Richards, J.M. & Morgan, R. (1991b): Geology and gold mineralization of the Omai property, Guyana. *Unpubl. rep.*

_____, _____, _____, Minamoto, J. & Richards, J.M. (1991a): Geology and gold mineralization of the Omai property, Guyana. *In* Brazil Gold '91: the Economic Geology Geochemistry and Genesis of Gold Deposits (E.A. Ladeira, ed.). Balkema, Rotterdam, The Netherlands (767-771).

Bowell, R.J., Foster, R.P. & Stanley, C.J. (1990): Telluride mineralization at Ashanti gold mine, Ghana. *Mineral. Mag.* **54**, 617-627.

Brown, A. & Lewis, B. (1962): The systems bismuth–tellurium and antimony–tellurium and the synthesis of the minerals hedleyite and wehrlite. *Phys. Chem. Solids* **23**, 1597-1604.

Cabri, L.J. (1965): Phase relations in the Au–Ag–Te system and their mineralogical significance. *Econ. Geol.* **60**, 1569-1606.

Clayton, R.N., O'Neil, J.R. & Mayeda, T.K. (1972) : Oxygen isotope exhange between quartz and water. *J. Geophys. Res.* **77**, 3057-3067.

Cooke, D.R., McPhail, D.C. & Bloom, M.S. (1996): Epithermal gold mineralization, Acupan, Baguio district, Philippines: geology, mineralization, and the thermochemical environment of ore deposition. *Econ. Geol.* **91**, 243-272.

Dobbe, R. (1993): Bismuth tellurides (joseite-B, bismuthian tsumoite) in a Pb–Zn deposit from Tunaberg, Sweden. *Eur. J. Mineral.* **5**, 165-170.

Elliott, R.G. (1992): *The Geology and Geochemistry of the Omai Goldfield, Guyana.* Ph.D. thesis, Oxford Brookes Univ., Oxford, U.K.

Fournier, R.O. & Truesdell, A.H. (1973): An empirical Na–K–Ca geothermometer for natural waters. *Geochim. Cosmochim. Acta* **37**, 1255-1275.

Garuti, G. & Rinaldi, R. (1986): Mineralogy of melonite-group and other tellurides from the Ivrea–Verbano basic complex, western Italian Alps. *Econ. Geol.* **81**, 1213-1217.

Gebre-Mariam, M., Groves, D.I., McNaughton, N.J., Mikucki, E.J. & Vearncombe, J.R. (1993): Archean Au–Ag mineralization at Racetrack, near Kalgoorlie, Western Australia: a high crustal-level expression of the Archean lode-gold system. *Mineral. Deposita* **28**, 375-387.

GIBBS, A.K. & BARRON, C.N. (1993): *Geology of the Guiana Shield*. Oxford University Press, Oxford, U.K.

GROVES, D.I. & FOSTER, R.P. (1991): Archean lode gold deposits. *In* Gold Metallogeny and Exploration (R.P. Foster, ed.). Blackie, London, U.K. (63-103).

HAGEMANN, S.G., GEBRE-MARIAM, M. & GROVES, D.I. (1994): Surface-water influx in shallow-level Archean lode-gold deposits in Western Australia. *Geology* **22**, 1067-1070.

HALLBAUER, D.K. (1994): Geochemical trace element analysis for ionic species by capillary electrophoresis. *Mineral. Mag.* **58A**, 362-363 (abstr.).

_____ & VOICU, G. (1998): A geochemical assessment of the hydrothermal systems at the Omai gold mine, Guyana, from the composition of fluid inclusions in ore minerals and gangue. *In* Geocongress '98, Geological Society of South Africa, Extended Abstr., 213-215.

HARRIS, D.C. (1989): The mineralogy and geochemistry of the Hemlo gold deposit, Ontario. *Geol. Surv. Can., Econ. Geol. Rep.* **38**.

_____, SINCLAIR, W.D. & THORPE, R.I. (1983): Telluride minerals from the Ashley deposit, Bannockburn Township, Ontario. *Can. Mineral.* **21**, 137-143.

HAYASHI, K. & OHMOTO, H. (1991): Solubility of gold in NaCl- and H_2S-bearing aqueous solutions at 250°–350°C. *Geochim. Cosmochim. Acta* **55**, 2111-2126.

HELGESON, H.C. (1969): Thermodynamics of hydrothermal systems at elevated temperatures and pressures. *Am. J. Sci.* **267**, 729-804.

HUDSON, D.R. (1986): Platinium-group minerals from the Kambalda nickel deposits, Western Australia. *Econ. Geol.* **81**, 1218-1225.

JAIRETH, S. (1991): Hydrothermal geochemistry of Te, Ag_2Te, and $AuTe_2$ in epithermal precious metal deposits. *James Cook Univ. of North Queensland, Australia, Econ. Geol. Res. Unit, Publ.* **37**.

JOHNSON, J.W., OELKERS, E.H. & HELGESON, H.C. (1992): SUPCRT92: a software package for calculating the standard molal thermodynamic properties of minerals, gases, aqueous species and reactions from 1 to 5000 bars and 0 to 1000°C. *Computers Geosci.* **18**, 899-947.

JOHNSTON, R. (1960): *The Geology of the Omai Mine, British Guyana*. Ph.D. thesis, Univ. of St. Andrews, St. Andrews, Scotland, U.K.

KELLY, W.C. & GODDARD, E.N. (1969): Telluride ores of Boulder County, Colorado. *Geol. Soc. Am., Mem.* **109**.

KUCHA, H., STUMPFL, E.F., PLIMER, I.R. & KÖCK, R. (1994): Gold–pyrite association – result of oxysulphide and polysulphide transport of gold? *Trans. Inst. Mining Metall.* **103**, B197-B205.

LEGENDRE, B., SOULEAU, C. & HANCHENG, CHHAY (1980): Le système ternaire or–argent–tellure. *Soc. Chim. Fr., Bull., partie* **1**, 197-204.

MCPHAIL, D.C. (1995): Thermodynamic proprieties of aqueous tellurium species between 25 and 350°C. *Geochim. Cosmochim. Acta* **59**, 851-866.

MILÉSI, J-P., LEDRU, P., FEYBESSE, J-L., DOMMANGET, A. & MARCOUX, E. (1992): Early Proterozoic ore deposits and tectonics of the Birimian orogenic belt, West Africa. *Precambrian Res.* **58**, 305-344.

O'NEIL, J.R., CLAYTON, R.N. & MAYEDA, T.K. (1969): Oxygen isotope fractionation in divalent metal carbonates. *J. Chem. Phys.* **51**, 5547-5558.

OZAWA, T. & SHIMAZAKI, H. (1982): Pilsenite redefined and wehrlite discredited. *Proc. Japan. Acad.* **58**, 291-294.

PHILLIPS, G.N. (1986): Geology and alteration in the Golden Mile, Kalgoorlie. *Econ. Geol.* **81**, 779- 808.

POHL, D.C. & BEATY, D.W. (1990): The mineralogy and petrology of telluride – sulfosalt – sulfide replacement deposits in the Leadville dolomite, Buckeye Gulch, Colorado. *Econ. Geol., Monogr.* **7**, 407-416.

RAO, N.K., NARASIMHAN, D. & RAO, G.V.U. (1980): The nickel telluride mineral melonite from the Jaduguda uranium deposit, Singhbhum shear zone, Bihar, India. *Mineral. Mag.* **43**, 775-777.

RIDLEY, J., MIKUCKI, E.J. & GROVES, D.I. (1996): Archean lode-gold deposits: fluid flow and chemical evolution in vertically extensive hydrothermal systems. *Ore Geol. Rev.* **10**, 279-293.

ROBERT, F. & BROWN, A.C. (1986): Archean gold-bearing quartz veins at the Sigma mine, Abitibi greenstone belt, Quebec. II. Vein paragenesis and hydrothermal alteration. *Econ. Geol.* **81**, 593-616.

SCHALAMUK, I.B. & LOGAN, A.M.V. (1994): Polymetallic Ag–Te-bearing paragenesis of the Cerro Negro district, Famatina Range, La Rioja, Argentina. *Can. Mineral.* **32**, 667-679.

SEWARD, T.M. (1991): The hydrothermal geochemistry of gold. *In* Gold Metallogeny and Exploration (R.P. Foster, ed.). Blackie, London, U.K. (37-62).

SHENBERGER, D.M. & BARNES, H.L. (1989): Solubility of gold in aqueous sulfide solutions from 150 to 350°C. *Geochim. Cosmochim. Acta* **53**, 269-278.

SHIMADA, N., MIYAHISA, M. & HIROWATARI, F. (1981): Melonite and volynskite from the Yokozuru mine, Sannotake, north Kyushu, Japan. *Mineral. J.* **10**, 269-278.

SIDDELEY, G. & ARANEDA, R. (1986): El Indio – Tambo gold deposits, Chile. *In* Gold '86 (A.J. Macdonald, ed.). Konsult International, Willowdale, Ontario (445-456).

THOMPSON, T.B., TRIPPEL, A.D. & DWELLEY, P.C. (1985): Mineralized veins and breccias of the Cripple Creek district, Colorado. *Econ. Geol.* **80**, 1669-1688.

TREMLOW, S.G. (1984): Archean gold–telluride mineralization of the Commoner mine, Zimbabwe. *In* Gold '82 (R.P. Foster, ed.). Balkema, Rotterdam, The Netherlands (469-492).

VOICU, G. (1999): *Geology, Geochemistry and Metallogeny of the Omai Gold Deposit, Guiana Shield, South America.* Ph.D. thesis, Univ. du Québec à Montréal, Montréal, Québec.

_____, BARDOUX, M., HARNOIS, L. & CRÉPEAU, R. (1997): Lithological and geochemical features of igneous and sedimentary rocks at the Omai gold mine, Guyana, South America. *Explor. Mining Geol.* **6**, 153-170.

WALROND, G.W. (1987): *Geological Map of Guyana* (scale 1:1 million). Guyana Geology and Mines Commission, Georgetown, Guyana.

WESOLOWSKI, D. & OHMOTO, H. (1986): Calculated oxygen isotope fractionation factors between water and the minerals scheelite and powellite. *Econ. Geol.* **81**, 471-477.

ZHANG, XIAOMAO & SPRY, P.G. (1994): Calculated stability of aqueous tellurium species, calaverite, and hessite at elevated temperatures. *Econ. Geol.* **89**, 1152-1166.

Received September 22, 1998, revised manuscript accepted April 10, 1999.